Planck-Weighted Transmittance and Correction of Solar Reflection for Broadband Infrared Satellite Channels

YONG CHEN

Cooperative Institute for Research in the Atmosphere, Colorado State University, Fort Collins, Colorado

FUZHONG WENG AND YONG HAN

NOAA/National Environmental Satellite, Data, and Information Service/Center for Satellite Applications and Research, Camp Springs, Maryland

QUANHUA LIU

Dell, Inc., Camp Springs, Maryland

(Manuscript received 10 June 2011, in final form 26 October 2011)

ABSTRACT

The line-by-line radiative transfer model (LBLRTM) is used to derive the channel transmittances. The channel transmittance from a level to the top of the atmosphere can be approximated by three methods: Planck-weighted transmittance 1 (PW1), Planck-weighted transmittance 2 (PW2), and non-Planck-weighted transmittance (ORD). The PW1 method accounts for a radiance variation across the instrument's spectral response function (SRF) and the Planck function is calculated with atmospheric layer temperature, whereas the PW2 method accounts for the variation based on the temperatures at the interface between atmospheric layers. For channels with broad SRFs, the brightness temperatures (BTs) derived from the ORD are less accurate than these from either PW1 or PW2. Furthermore, the BTs from PW1 are more accurate than these from PW2, and the BT differences between PW1 and PW2 increase with atmospheric optical thickness.

When the band correction is larger than 1, the PW1 method should be used to account for the Planck radiance variation across the instrument's SRF. When considering the solar contribution in daytime, the correction of the solar reflection has been made for near-infrared broadband channels ($\sim$3.7 μm) when using PW1 transmittance. The solar transmittance is predicted by using explanatory variables, such as PW1 transmittance, the secant of zenith angle, and the surface temperature. With this correction, the errors can be significantly reduced.

1. Introduction

The development of fast and accurate thermal infrared (IR) radiative transfer (RT) models for clear atmospheric conditions has enabled the direct assimilation of satellite-based radiance measurements in numerical weather prediction (NWP) models. Most fast RT models are based on fixed transmittance coefficients that relate atmospheric conditions to optical properties. One such fast RT model is the Community Radiative Transfer Model (CRTM; Weng et al. 2005; Han et al. 2006; Chen et al. 2008), which has been developed at the Joint Center for Satellite Data Assimilation (JCSDA) and used to simulate satellite radiances in the Global Forecast System (GFS) at the National Centers for Environmental Prediction (NCEP). To generate the CRTM transmittance coefficients, the regression algorithms (Chen et al. 2010; McMillin et al. 2006) are solved by using diverse profiles of temperature, water vapor, ozone, and the corresponding transmittance computed from a line-by-line (LBL) spectroscopy model. The 83 profiles provided by the European Centre for Medium-Range Weather Forecasts (ECMWF; Chevallier et al. 2006) and the 48 profiles provided by the University of Maryland, Baltimore County (UMBC; Strow et al. 2003), are representative of the range of variations in temperature and absorber amount found in the real atmospheres. In the regression algorithm, the LBL transmittances convolved with

Corresponding author address: Yong Chen, 5200 Auth Road, Room 703, Camp Springs, MD 20746.
E-mail: yong.chen@noaa.gov

DOI: 10.1175/JTECH-D-11-00102.1

spectral response functions (SRFs) are predictands and the atmospheric variables are predictors. There can be as many as 15 predictors for the water vapor transmittance (see Table 1 in Chen et al. 2010). The convolution of the LBL transmittance with the instrument's SRF is referred to as the channel transmittance. The basic assumption in the channel transmittance calculation is that either the Planck function does not change with wavenumber, or the change is negligible when the satellite radiance is simulated by integrating the radiance at the top of the atmosphere within the wavenumber domain covered by the instrument spectral response function. In this paper, the transmittance resulting from this convolution is referred to as the non-Planck-weighted transmittance (PW), or the ordinary transmittance (ORD). Previously, the channel transmittance that was used by the CRTM was calculated without accounting for the change in Planck radiances across the spectra of SRFs. This approximation is less valid for wide spectral bands where the Planck radiance changes significantly with wavenumber. In previous studies, simulations of the Spinning Enhanced Visible and Infrared Imager (SEVIRI) 3.9-μm channel, using another fast RT model known as the radiative transfer for Television and Infrared Observation Satellite (TIROS) Operational Vertical Sounder (RTTOV; Saunders et al. 1999; Matricardi 2008), were shown to be significantly more accurate when weighting the channel transmittance calculations based on the Planck radiance variation (Brunel and Turner 2003).

Because the PW methods implicitly account for the atmospheric temperature through the Planck function in the channel transmittance calculation, the vertical resolution of the atmospheric profile plays an important role in determining the accuracy of the convolved channel transmittance. In a fast RT model the input atmospheric profile is usually divided into a finite number of layers for efficient computation. However, the radiances or brightness temperatures simulated using fast models become less accurate when either the vertical temperature variation increases or the layer optical thickness increases (Chou and Lee 2005).

In this study, we investigate the accuracy of radiance simulations for two techniques that are used to calculate the Planck-weighted transmittances. One uses the layer temperature to account for Planck radiance variation, and the other uses the level temperature at the interface of the layer boundaries. Radiance simulations for a hypothetical sensor containing five channels that have spectral bandwidths located at different absorption bands are analyzed. The first channel of the five-channel set is the same as channel 8 of the Geostationary Operational Environmental Satellite (GOES)-R Advanced Baseline Imager (ABI), the second channel is the same as the *National Oceanic and Atmospheric Administration* (*NOAA*)-*16* Advanced Very High Resolution Radiometer (AVHRR)/3 channel 3, the third channel is the same as *GOES-12*'s channel 15, and the fourth and fifth channels are the same as the *Meteorological Satellite* (*Meteosat*)-*9* SEVIRI's channels 4 and 11, respectively. The hypothetical sensor channels 1 and 4 have similar central wavenumbers, but channel 4 has the largest bandwidth. Channel 2 is unique because of its out-of-band SRF (Liu et al. 2009). Channels 3 and 5 are located within CO_2 absorption bands, but channel 3 is relatively narrow. The characterizations of the five channels are shown in Table 1.

Because the Planck-weighted channel transmittance accounts for the Planck function evaluated at atmospheric temperatures, it is not suitable for calculations of the solar contribution from surface reflection during the daytime. The difference between the solar channel transmittance and the Planck-weighted channel transmittance must be considered in order to accurately calculate the thermal infrared radiance as well as the solar reflection radiance for the satellite near-infrared (NIR) channels.

This paper is organized as follows. Section 2 describes three approximation methods used in the fast model to estimate channel transmittances. Section 3 compares LBL and fast RT model calculations for the three approximation methods. In section 4, the sensitivity of the results from the three methods to the atmospheric profiling schemes is presented. Section 5 discusses the correction of solar reflection for NIR channels when using PW transmittance. Finally, section 6 summarizes the conclusions of this study.

2. Infrared radiative transfer and approximations for channel transmittance

The general radiative transfer equation used to model the upward radiation at top of the atmosphere (TOA) under cloud-free conditions can be expressed as

$$R_\nu = \varepsilon_\nu B_s[\nu, T(z_s)]\tau(\nu, z_s) + (1 - \varepsilon_\nu)\tau(\nu, z_s)\int_1^{\tau(\nu,z_s)} B[\nu, T(z)]\, d\tau(\nu, z) + \int_{\tau(\nu,z_s)}^1 B[\nu, T(z)]\, d\tau(\nu, z) + r\mu_0 F_* \tau(\nu, z_s, \mu_0)\tau(\nu, z_s, \mu)/\pi, \quad (1)$$

TABLE 1. Characteristics of the five channels used in this study. The BT band correction coefficients are calculated using Eq. (11) for a temperature range from 180 to 340 K.

Pseudochannel	Satellite sensor	Spectral interval (cm^{-1})	Central wavenumber (cm^{-1})	BT band correction coefficients		
				b	b_1	RMS
1	N/A	2456.0–2683.3	2563.790	4.9724×10^{-1}	9.9929×10^{-1}	2.9985×10^{-4}
2	*NOAA-16* AVHRR/3 channel 3	2222.7–3355.7	2697.562	2.2687×10^{0}	9.9642×10^{-1}	1.5148×10^{-2}
3	*GOES-12* sounder channel 15	2225.8–2271.1	2248.638	2.0287×10^{-2}	9.9997×10^{-1}	2.4825×10^{-5}
4	*Meteosat-9* SEVIRI channel 4	2083.3–3289.5	2568.259	3.3855×10^{0}	9.9540×10^{-1}	4.5146×10^{-3}
5	*Meteosat-9* SEVIRI channel 11	649.4–877.2	750.660	3.1222×10^{-1}	9.9869×10^{-1}	6.8775×10^{-3}

where ν is the wavenumber, z is the height, B is the Planck function, the subscript s denotes the surface, T is the temperature, and τ is the transmittance. Respectively, ε_ν, r, μ_0, μ, and F_* are surface emissivity, surface reflectivity, secant of solar zenith angle, secant of satellite zenith angle, and solar irradiance. The first three terms account for the thermal infrared or microwave contribution (e.g., surface emission, surface-reflected downward atmospheric emission, and upward atmospheric emission), and the last term accounts for direct solar reflection. To simplify this radiative transfer problem, we assume a surface emissivity of 1, and the upward infrared radiation at TOA becomes

$$R_\nu = B_s[\nu, T(z_s)]\tau(\nu, z_s) + \int_{\tau(\nu,z_s)}^{1} B[\nu, T(z)]\, d\tau(\nu, z). \tag{2}$$

The channel radiance received by the satellite sensor is computed by convolving the monochromatic radiances with the instrument SRF within the channel interval $\Delta\nu$ (from the beginning wavenumber ν_1 to the ending wavenumber ν_2) as

$$R = \frac{\int_{\Delta\nu} \phi(\nu) B_s[\nu, T(z_s)]\tau(\nu, z_s)\, d\nu + \int_{\Delta\nu} \phi(\nu) \int_{\tau(\nu,z_s)}^{1} B[\nu, T(z)]\, d\tau(\nu, z)\, d\nu}{\int_{\Delta\nu} \phi(\nu)\, d\nu}, \tag{3}$$

where $\phi(\nu)$ is the spectral response function of a channel.

To approximate the integral in Eq. (3), the atmosphere is divided into N layers ($N + 1$ levels), numbered incrementally from TOA to the surface as shown in Fig. 1. There are two forms of vertical discretization for the second term in Eq. (3)—one is to use integration by parts $\tau(\nu, z)\, dB[\nu, T(z)]$, the other is $B[\nu,T(z)]\, d\tau(\nu, z)$. The first one involves effective transmittance from TOA to layer i, and the second one involves effective transmittance from TOA to level i. In this study, we used the second approach because of the fact that the level-to-space (or level to TOA) transmittance is commonly used in fast RT models. After the discretization in the vertical direction, the channel radiance becomes

$$R \approx \frac{\int_{\Delta\nu} \phi(\nu) B_s[\nu, T(z_s)]\tau(\nu, z_s)\, d\nu + \sum_{i=1}^{N} \int_{\Delta\nu} \phi(\nu) \overline{B[\nu, T_i]}[\tau(\nu, z_{i-1}) - \tau(\nu, z_i)]\, d\nu}{\int_{\Delta\nu} \phi(\nu)\, d\nu}, \tag{4}$$

where $\overline{B[\nu, T_i]}$ is the effective Planck function of a layer between the levels $i - 1$ and i, which is taken to be the Planck function of the mean layer temperature (the average value between the top and bottom levels of the layer) $B[\nu, \overline{T}_i]$ in this study [more discussion of effective Planck function of a layer can be seen in Chou and Lee (2005)], and $\tau(\nu, z_i)$ is the transmittance between the TOA and level i. Because the Planck function is a function of wavenumber, Eq. (4) can be rewritten as

$$R = \frac{\int_{\Delta\nu}\phi(\nu)B_s[\nu,T(z_s)]\,d\nu}{\int_{\Delta\nu}\phi(\nu)\,d\nu}\frac{\int_{\Delta\nu}\phi(\nu)B_s[\nu,T(z_s)]\tau(\nu,z_s)\,d\nu}{\int_{\Delta\nu}\phi(\nu)B_s[\nu,T(z_s)]\,d\nu}$$
$$+\sum_{i=1}^{N}\frac{\int_{\Delta\nu}\phi(\nu)\overline{B[\nu,T_i]}\,d\nu}{\int_{\Delta\nu}\phi(\nu)\,d\nu}\left\{\frac{\int_{\Delta\nu}\phi(\nu)\overline{B[\nu,T_i]}\tau(\nu,z_{i-1})\,d\nu}{\int_{\Delta\nu}\phi(\nu)\overline{B[\nu,T_i]}\,d\nu}-\frac{\int_{\Delta\nu}\phi(\nu)\overline{B[\nu,T_i]}\tau(\nu,z_i)\,d\nu}{\int_{\Delta\nu}\phi(\nu)\overline{B[\nu,T_i]}\,d\nu}\right\}$$
$$\approx\frac{\int_{\Delta\nu}\phi(\nu)B_s[\nu,T(z_s)]\,d\nu}{\int_{\Delta\nu}\phi(\nu)\,d\nu}\tau_s+\sum_{i=1}^{N}\frac{\int_{\Delta\nu}\phi(\nu)B[\nu,\overline{T_i}]\,d\nu}{\int_{\Delta\nu}\phi(\nu)\,d\nu}(\tau_{i-1}-\tau_i). \quad (5)$$

To obtain the channel transmittance coefficients that are used to predict the optical depth in fast models (such as CRTM and RTTOV), the common approach is to convolve the transmittances calculated from the line-by-line model with the instrument SRF. The transmittances resulting from this basic convolution are referred to as ordinary transmittances, whereas the Planck-weighted transmittances take into account the variation of the Planck radiance for each channel spectral interval. Because of the requirements of fast RT models, the channel transmittance must be continuous at the interface of layers for efficient computation and less memory storage. To predict the layer optical depth, the second term in Eq. (5), which includes transmittance, cannot be directly used because of the two sets of transmittances existing at the interface. For the level i transmittance one involves the i layer Planck function, and the other includes the $i + 1$ layer Planck function. Based on different assumptions and approximations, the channel transmittance τ_i in Eq. (5) can be applied three different ways in fast radiative transfer models.

In approximation 1 (referred to as PW1), the layer temperature is used to calculate the Planck-weighted channel transmittance as

$$\tau_i^{\mathrm{PW1}} = \frac{\int\phi(\nu)B[\nu,\overline{T_i}]\tau_i(\nu)\,d\nu}{\int\phi(\nu)B[\nu,\overline{T_i}]\,d\nu}. \quad (6)$$

In approximation 2 (referred to as PW2), the level temperature is used to calculate the Planck-weighted channel transmittance as

$$\tau_i^{\mathrm{PW2}} = \frac{\int\phi(\nu)B[\nu,T_i]\tau_i(\nu)\,d\nu}{\int\phi(\nu)B[\nu,T_i]\,d\nu}. \quad (7)$$

In approximation 3 (referred to as ORD), the variation of the Planck radiances within the channel spectra is not considered when calculating channel transmittance,

$$\tau_i^{\mathrm{ORD}} = \frac{\int\phi(\nu)\tau_i(\nu)\,d\nu}{\int\phi(\nu)\,d\nu}. \quad (8)$$

For thermal infrared radiation, it is common for channel radiance to be represented as a channel brightness temperature (BT). There are three standard approaches for representing radiance as BT (Berk 2008). The simplest algorithm uses the Planck function to convert radiance to BT at the channel's central wavenumber. This approach is not accurate for temperatures far away from the standard temperature (273.15 K). Iterative approaches for determining the BT that calculates the radiance integrated over the SRF are sufficiently accurate, but these approaches are computationally inefficient. The fast and practical way to convert channel radiance to channel BT is to use band correction at the channel central wavenumber with empirical fits of BT versus radiance (Weinreb et al. 1981). These parameterization processes are sufficiently accurate and computationally efficient. The channel central wavenumber ν_i is defined as the first spectral moment of the SRF

$$\nu_i = \frac{\int_{\Delta\nu}\phi(\nu)\nu\,d\nu}{\int_{\Delta\nu}\phi(\nu)\,d\nu}. \quad (9)$$

For each channel, the channel effective brightness temperature T_e at the center wavenumber ν_i is calculated for the blackbody temperature T over the instrument channel SRF,

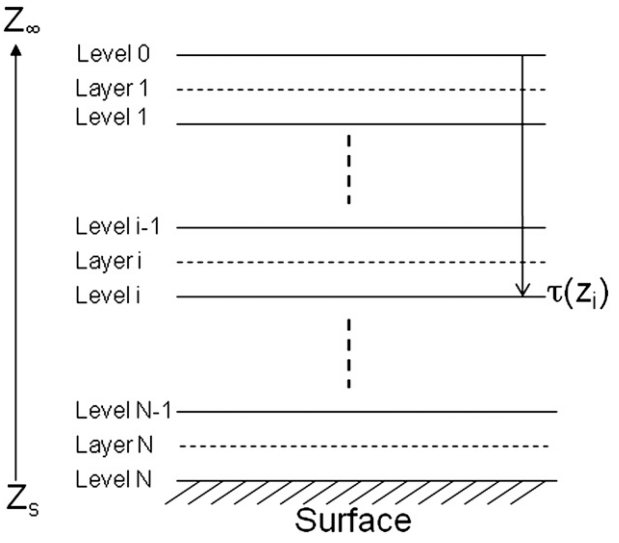

FIG. 1. The vertical layer scheme for an atmosphere consisting of N layers ($N + 1$ levels).

$$R = \frac{c_1 \nu_i^3}{e^{c_2 \nu_i / T_e} - 1} = \frac{\int_{\Delta\nu} \phi(\nu) B[\nu, T]\, d\nu}{\int_{\Delta\nu} \phi(\nu)\, d\nu}, \qquad (10)$$

where c_1 and c_2 are the Planck function constants. A linear relationship between T and T_e is established by ranging T from 180 to 340 K,

$$T = (T_e - b)/b_1, \qquad (11)$$

where b and b_1 are the fitting coefficients (band correction coefficients). For a given radiance R, the channel BT T can be quickly and accurately obtained by calculating T_e using Eq. (10) and then applying Eq. (11). We should note that this band correction is different from the PW channel transmittance calculation. However, the band correction coefficient b is a very good indicator for Planck radiance variation across the channel SRF. For IR channels that have a very broad SRF and a large Planck radiance variation across the instrument SRF for terrestrial temperatures, the coefficient b tends to be large. Table 1 contains the fitting coefficients for the five channels used in this study. Note that the correction coefficients b for channels 2 and 4 are 2.2687 and 3.3855, respectively. These band correction coefficients are used to perform radiance-to-BT conversions at the channel's central wavenumber for all of the approximation methods and LBL.

3. Comparison results

A UMBC dataset that contains 48 diverse atmospheric profiles with 101 pressure levels (Strow et al. 2003) was selected for this study. The first five are standard climatological profiles (tropical, midlatitude summer, midlatitude winter, subarctic summer, and subartic winter). The 101 pressure levels are fixed based on the AIRS science team definition (Strow et al. 2003; Saunders et al. 2007),

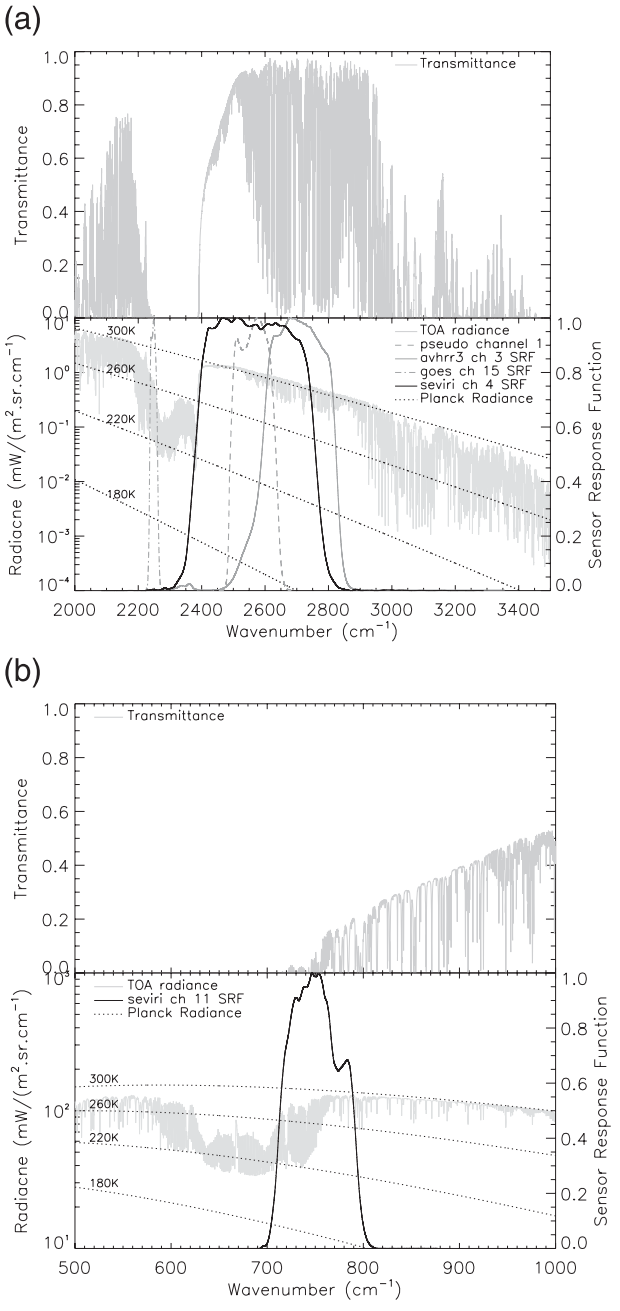

FIG. 2. Channel spectral response functions for (a) a pseudochannel, *NOAA-16* AVHRR/3 channel 3, *GOES-12* channel 15, and *Meteosat-9* SEVIRI channel 4 and (b) SEVIRI channel 11. (top) The surface-to-space transmittance, TOA radiance for tropical model atmosphere, and (bottom) theoretical Planck radiance curves for a number of atmospheric temperatures are also shown in (a),(b).

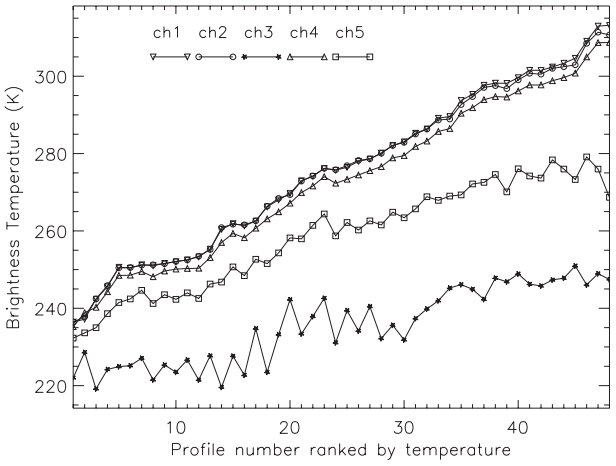

FIG. 3. The line-by-line brightness temperatures as a function of profile number ranked by temperature for the UMBC 48 diverse atmospheric profiles.

$$P_{\text{lev}}(i) = (Ai^2 + Bi + C)^{7/2}, \tag{12}$$

where i is the level number, and A, B, and C are constants.

In this study, version 11.3 of the line-by-line radiative transfer model (LBLRTM; Clough et al. 2005) was used to simulate monochromatic level-to-space transmittances. The spectroscopic database used in LBLRTM is a version

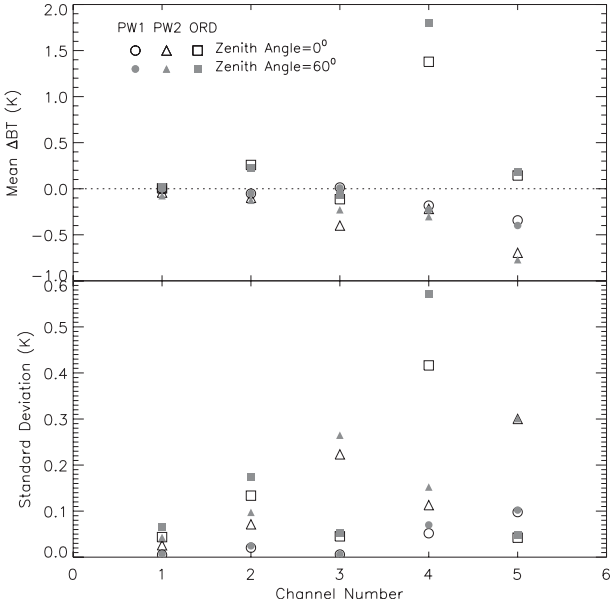

FIG. 4. Mean brightness temperature differences and standard deviations for approximation methods PW1, PW2, and ORD compared to LBL results for the UMBC 48 diverse atmospheric profiles at nadir.

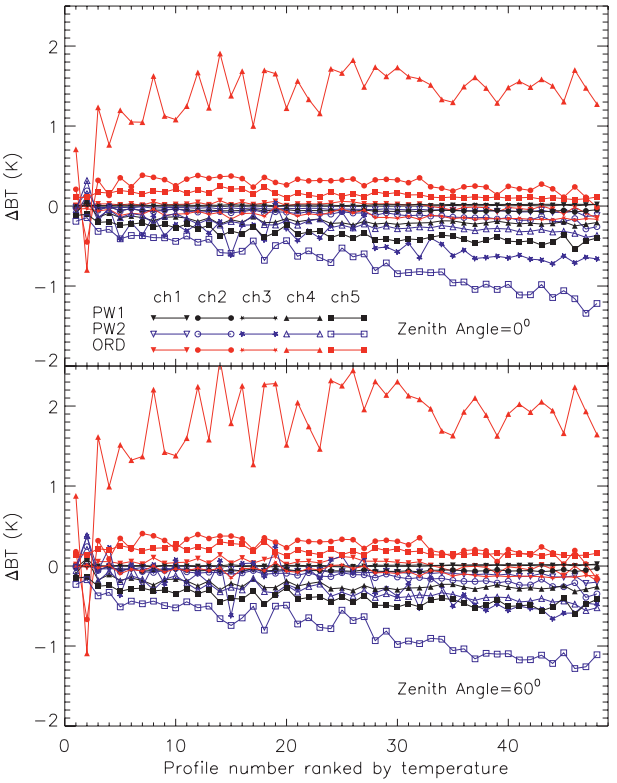

FIG. 5. The brightness temperature differences for approximation methods PW1, PW2, and ORD compared to LBL calculation as a function of profile number ranked by temperature for the UMBC 48 diverse atmospheric profiles at (top) nadir and (bottom) 60°.

of High Resolution in Transmission (HITRAN) 2004, which includes Atmospheric and Environmental Research (AER) version 2.1 updates. The spectral resolution for the channel SRF is set to 1×10^{-3} cm^{-1}. The variable gases for the input profiles include H_2O, CO_2, and O_3. All of the other gas profiles are fixed in the transmittance calculations.

Based on the above three convolved transmittances, the clear-sky channel radiances can be calculated. We compare the fast model BTs to the LBL results for the five channels. The SRFs for the five channels are shown in Figs. 2a,b. The surface-to-space transmittance, TOA radiance, and theoretical Planck radiances for several atmospheric temperatures (180, 220, 260, and 300 K) are also displayed. *Meteosat-9* SEVIRI channel 4 and *NOAA-16* AVHRR/3 channel 3 have very broad channel responses, from 2083 to 3289 cm^{-1} and from 2222 to 3355 cm^{-1}, respectively. Within the spectral intervals of those two channels, the Planck radiance changes by an order of magnitude, from 0.003 to 0.03 mW m^{-2} sr cm^{-1} for a temperature of 220 K. Compared with the NIR (from 2000 to 3500 cm^{-1}), the variation of the Planck

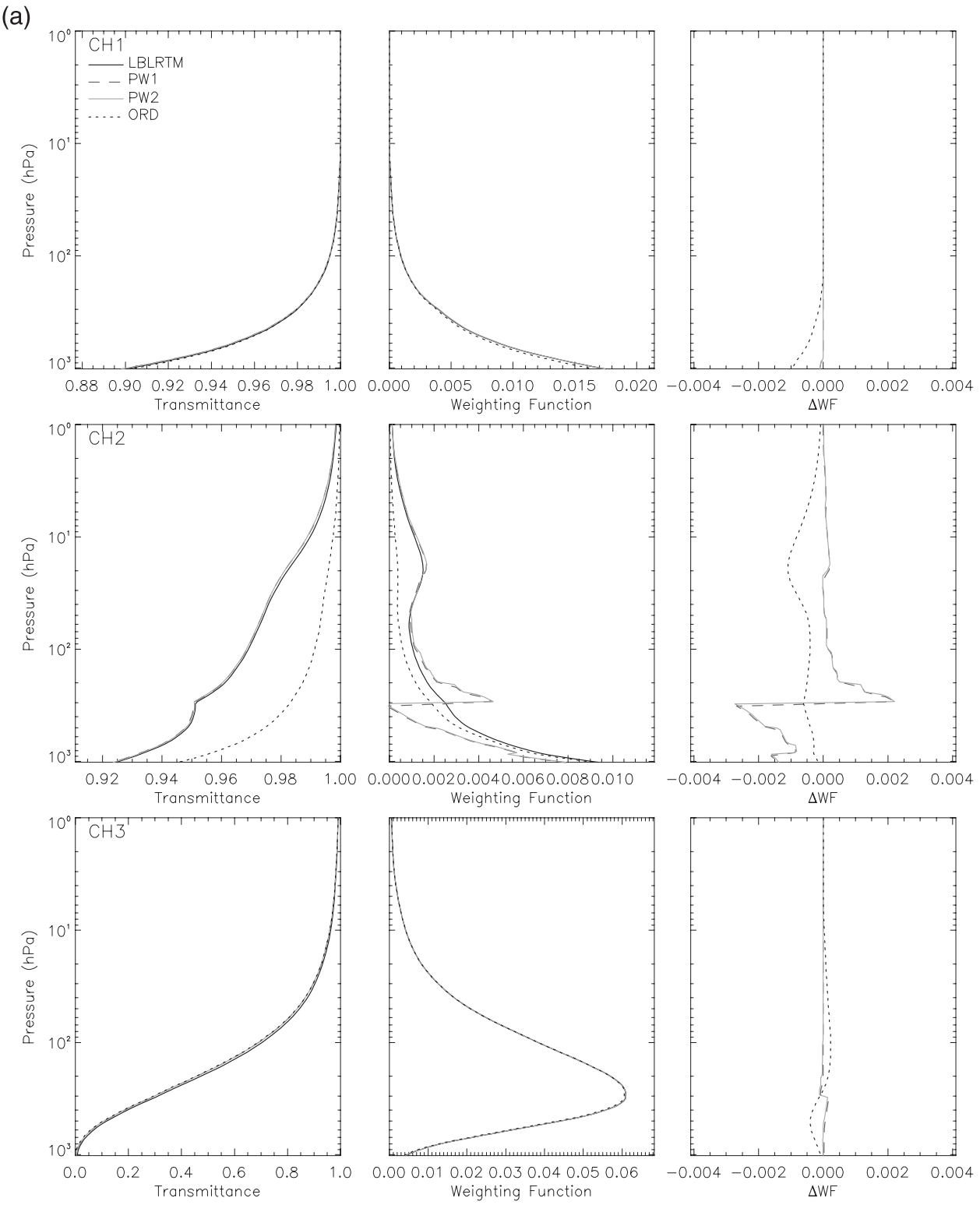

FIG. 6. Transmittance, weighting function, and weighting function difference profiles for approximation methods compared to LBLRTM results for the UMBC atmospheric profile number 10 for channels (a) 1–3 and (b) 4 and 5.

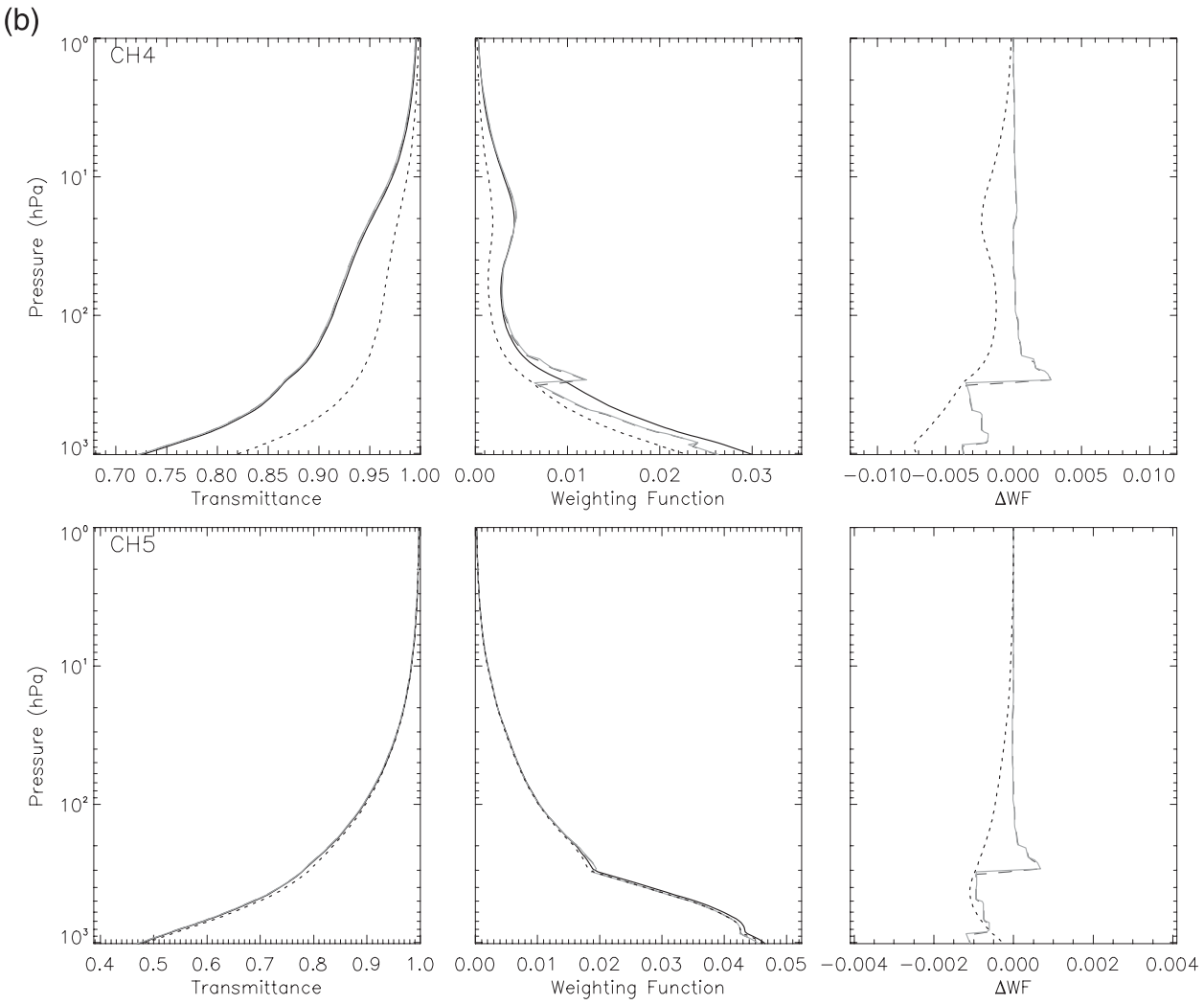

FIG. 6. (*Continued*)

radiance with wavenumber is relatively small in the middle IR (MIR; see Fig. 2b Planck radiance curves).

Figure 3 shows the five-channel brightness temperatures derived from the LBL calculations for UMBC atmospheric profiles as a function of profile number ranked by surface temperatures. Channels 1, 2, and 4 can be considered window channels, although channels 2 and 4 have a small bump in their SRF near the strong 4.3-μm CO_2 absorption band. Channel 3 is located in the strong 4.3-μm CO_2 absorption band, while channel 5 is a temperature sounding channel.

Figure 4 shows the mean and standard deviation of BT differences (ΔBT) between the fast model calculations and the LBL-derived calculations for sensor zenith angles of 0° and 60°. The BT differences for the PW1 method are smaller than those for the PW2 method for all channels. The BT differences when applying the ORD method are smaller than the BT differences for both PW methods for channels 1, 3, and 5. However, for channels 2 and 4, the BT differences for the ORD method are larger than the BT differences for both PW methods, especially for channel 4 (an around 2-K difference). The standard deviations of the BT differences for those two channels are also larger for the ORD method compared to the PW methods. Figure 5 shows the individual profile departures from the LBL results for the three methods as a function of profile number ranked by surface temperature. The BT differences (departure from LBL results) for the Planck-weighted transmittance methods have a stronger dependence on profile surface temperature than the ORD method. The ΔBT for both PW methods increases with surface temperature because the lapse rates in the tropopause are generally stable and the temperature differences between the atmospheric levels increase with surface temperature. Also, the optical thickness of the atmospheric

layers increases with surface temperature. The PW2 ΔBT are greater than those for the PW1 method. There is no relationship between ΔBT and surface temperature for the ORD method.

To better understand the results for the three methods, the transmittance and weighting function (defined as $W = [\tau(z_i) - \tau(z_{i+1})]/dz$) profile for a selected atmospheric profile are analyzed. The LBL transmittances are calculated from Eq. (5) before approximation, which is different from ORD and PW approximations. We chose profile number 10, which has a surface temperature of 277.2 K (with tropopause at 300 hPa). The surface temperature of profile 10 is the 25th coldest profile in the set. The comparison results are shown in Fig. 6. Because channel 1 is located in the spectroscopy window region, the weighting function peaks at the surface. The differences for the transmittance and weighting function between the LBL-derived calculations and those for the three methods are very small. A small negative weighting function difference near the surface is found for the ORD method resulting from the Planck radiance variation across the instrument SRF. For this channel, the three methods can produce accurate weighting function results, as shown in Figs. 4 and 5, because their transmittances are almost the same. The weighting function for channel 3 peaks at around 300 hPa regardless of the atmospheric profile. The weighting function for the ORD method is slightly larger than the LBL-derived result above the peak and smaller than the LBL-derived results below the peak. The features are opposite for PW1 and PW2. Although channels 2 and 4 are window channels that have the weighting functions peaking at the surface, they also have a secondary peak at around 20 hPa, because their SRFs are within the 4.3-μm CO_2 absorption band. For these two channels, the transmittance profiles for PW1 and PW2 are very similar to the LBL profiles, while the ORD transmittance profiles are larger at all levels. Because the Planck radiance is larger at the smaller wavenumbers (see Fig. 2a), the weighting of the transmittance for the portion of strong CO_2 absorption (i.e., the level-to-space transmittance is less than those from the window range) increases for the PW-weighted transmittances relative to the ORD transmittances. Transmittances calculated from Eqs. (6) and (7) are smaller than those calculated from Eq. (8). The secondary peak is absent in the ORD transmittances for channels 2 and 4. Both PW1 and PW2 weighting functions contain a secondary peak (note that LBL also presents a secondary peak), and they also show large differences at the tropopause near 300 hPa. Because temperature increases with height above the tropopause, the PW1 and PW2 methods increase the weighting function. Below the tropopause where temperature decreases with height, the two Planck-weighted methods have smaller weighting functions in comparison to those for the LBL-derived results. The shape of the weighting function profiles for PW1 and PW2 are similar, but the values are not the same for the same height (shifting one layer). The Planck-weighted methods alter the transmittance weighting function relative to those for the ORD method. The ORD method weighting functions have larger negative differences at the surface for channel 4. Compared to the LBL-derived results, channels 2 and 4 have smaller weighting function profiles at all levels when applying the ORD method. Channel 5 has a smaller weighting function difference in comparison to channel 2 and channel 4. However, the weighting function redistribution for channel 5 is similar to that for channels 2 and 4.

4. Sensitivity to atmosphere levels (layers)

The weighting function profile patterns for PW1 and PW2 are very similar. However, the BT differences for PW1 and PW2 are significant, and they increase with the surface temperature resulting from the temperature variations in the lower troposphere. Because we use the atmospheric layer or level temperature to modify the level transmittance in PW methods, the accuracy of the emission depends on the temperature difference between the layers (levels). If the atmosphere could be divided into an infinite number of layers (levels), the PW1 and PW2 transmittances would be identical. To test the sensitivity of the PW methods to the vertical resolution of the atmospheric profile, three types of layer schemes are used. In addition to the 101 level (referred to as LVL101) UMBC profiles, we also use profiles that are characterized with 66 levels (referred to as LVL66) and 28 levels (referred to as LVL28; see Fig. 7). The LVL66 and LVL28 profile sets have TOA pressures of 0.005 hPa and surface pressures of 1100 hPa. The LVL66 and LVL28 pressure levels were chosen to be the same as those of the typical output atmospheric profiles from the GFS developed at NCEP. The temperature and atmospheric absorber amounts in the LVL66 and LVL28 profiles are assumed to vary linearly with the logarithm of pressure and are interpolated from the LVL101 profile set.

To demonstrate the impact of the resolution of vertical levels on simulated BTs, we separate out differences resulting from the vertical resolution of the atmosphere from those resulting from polychromatic effects by defining a double BT difference as

$$\Delta BT = (BT - BT_{LBL}) - (BT_{ref} - BT_{ref\_LBL}), \quad (13)$$

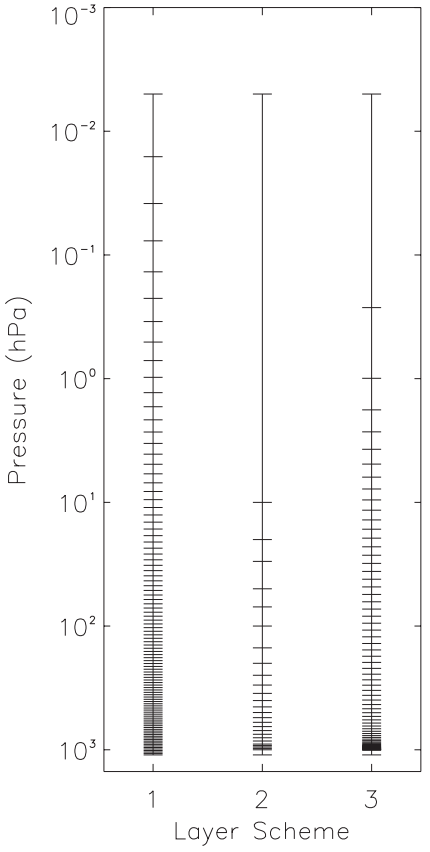

FIG. 7. Three layer schemes used to test the sensitivity of the approximation methods.

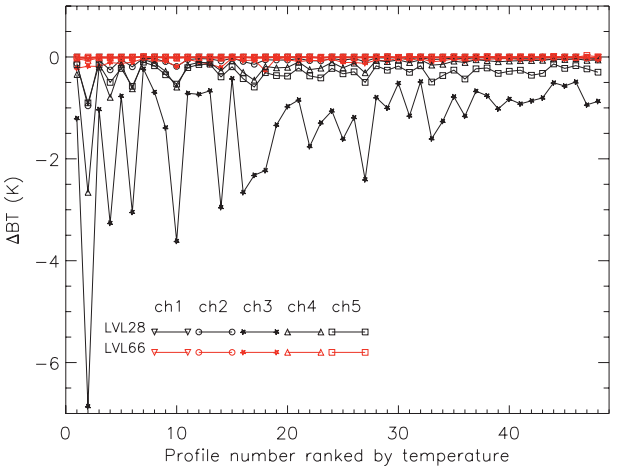

FIG. 8. LBL BT differences between LVL28 and LVL101, and between LVL66 and LVL101 as a function of profile numbers at nadir.

where BT is the brightness temperature using the LVL28 or LVL66 profile sets, BT_{ref} is the brightness temperature using the LVL101 profile set and applying the approximation methods, and the subscript LBL refers to the LBL results. The double BT differences provide information about how the accuracy of applying approximation methods relates to the difference of the vertical resolution of the atmosphere. In other words, this variable shows how closely the approximation methods agree with the LBL-derived results. Figure 8 shows the LBL BT differences between the LVL28 and LVL101 results and between the LVL66 and LVL101 results as a function of profile number at nadir. The BT differences are less than 0.2 K for the LVL66. However, the differences increase dramatically for the LVL28 profile set because of the atmospheric absorption above 10 hPa, which has an impact on the TOA brightness temperature (see the weighting function profile from Fig. 6), but the LVL28 profile set has only one layer above 10 hPa (see Fig. 7). Figure 9 shows the double BT differences for the PW1, PW2, and ORD methods at zenith angles of 0° and 60°. For all channels, the PW1 differences are smaller than 0.1 K (with only one profile greater than it). The double BT differences are significantly smaller for the PW1 method compared to those for the PW2 and ORD methods regardless of which layer scheme is used. The PW2 method shows increasingly negative double BT differences for coarse atmospheres and warmer surface temperatures. Large negative differences are shown for all of the channels, especially for channels 3 and 5 (which are greater than 0.5 K). The ORD method differences are relatively small for channels 1, 3, and 5. For channels 2 and 4, the ORD BTs are generally greater than the LBL results (see Fig. 5). The double BT differences for the ORD method are larger for coarse atmospheric profiles.

Based on the above-mentioned simulations and comparisons, the PW1 method should be applied for cases where the band correction coefficient b is greater than 1. The PW1 method accounts for the Planck radiance variation across the spectra of transmittances that span the instrument SRFs. This significantly reduces the BT biases relative to what is the case when applying the ORD method. Table 2 shows 16 broadband satellite sensor channels that have central wavenumbers ranging from 2500 to 2700 cm^{-1} for which we recommend using Planck-weighted transmittances for thermal IR radiation calculations. The mean BT differences and standard deviations between the three approximation methods and the LBL-derived results at zenith angles 0° and 60° for these 16 channels are shown in Fig. 10 for reference.

5. Correction of solar reflection for NIR channels when using PW transmittance

For the radiance calculation during daytime, the solar contribution from the surface reflection (the fourth term) in Eq. (1) for the NIR channels must be taken into

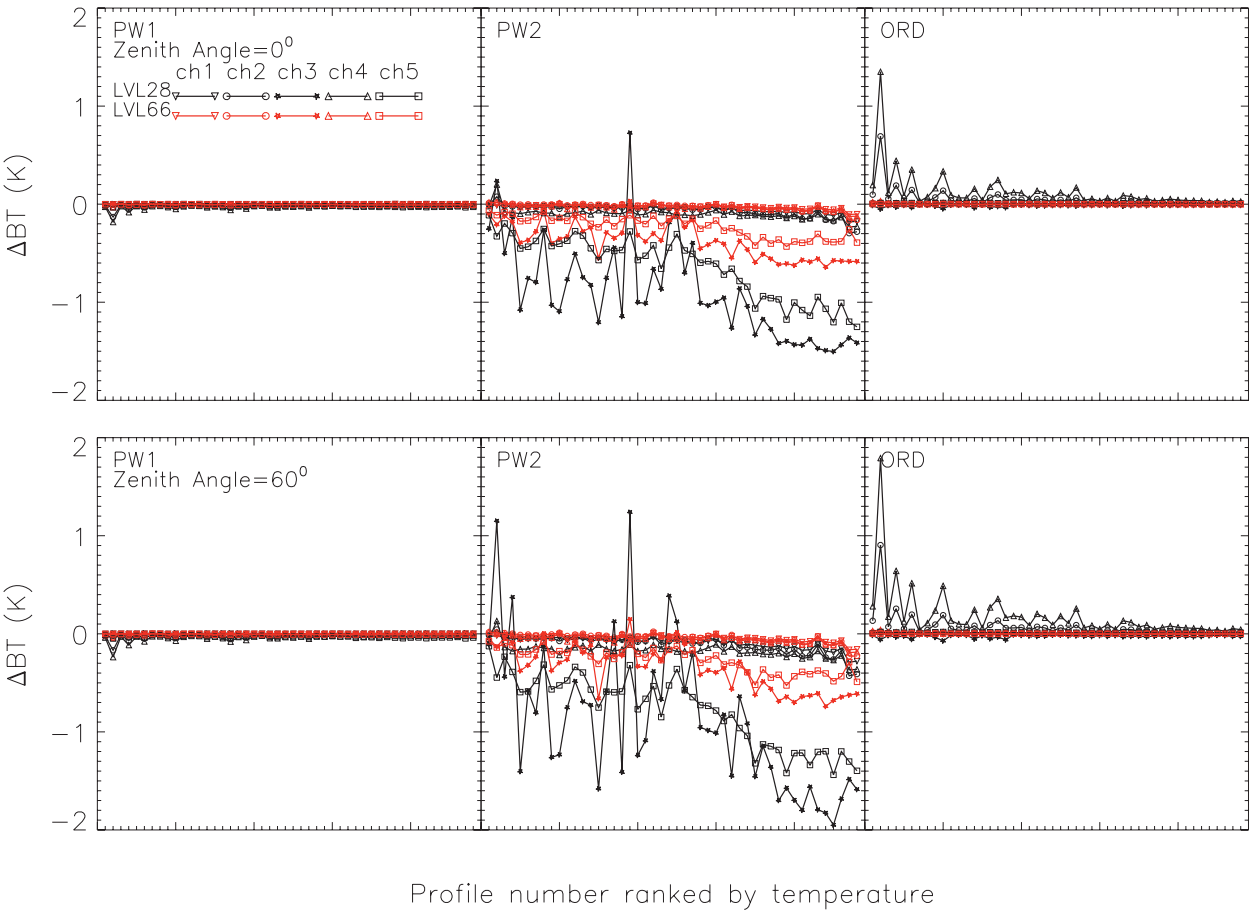

FIG. 9. The double brightness temperature differences (see text) for approximation methods PW1, PW2, and ORD.

account. The PW1 method can only be applied for thermal IR radiative transfer, and fast RT models can only have one total transmittance. The solar channel transmittance is defined as

$$\tau_i^s = \frac{\int \phi(\nu) R_s(\nu) \tau_i(\nu)\, d\nu}{\int \phi(\nu) R_s(\nu)\, d\nu}, \tag{14}$$

where R_s is the solar radiance and $\tau_i(\nu)$ is the monochromatic transmittance of the atmosphere at frequency ν. In principle, the solar transmittance could be estimated with the same method that is applied to compute the PW1 transmittance with the solar radiance as weights in the channel spectral convolution. In practice, the following expression can be used to estimate the error incurred in the clear-sky solar reflection contribution resulting from using the stored transmittance coefficients rather than the actual solar transmittance:

$$\Delta R_{\text{sol}} = r\mu_0 F_* \tau^{\text{PW1}}(\mu_0)\tau^{\text{PW1}}(\mu)/\pi - r\mu_0 F_* \tau^s(\mu_0)\tau^s(\mu)/\pi. \tag{15}$$

One straightforward approach to account for this difference is to predict the total solar transmittance by using known parameters in fast RT models. We used a multiple linear regression method to predict the total solar transmittance, with explanatory variables such as the PW1 total transmittance τ^{PW1}, secant of zenith angle μ, and lowest-level temperature T_s,

$$\tau_m^s = \beta_0 + \beta_1 \tau_m^{\text{PW1}} + \beta_2 \mu_m + \beta_3 (T_s)_m, \quad \text{for } m = 1, 2, \ldots, M, \tag{16}$$

where β_0, β_1, β_2, and β_3 are regression coefficients, and M is the total number of regression points. For the regression coefficients, 10 pairs of solar zenith angles and sensor zenith angles are used. The secants of the zenith angles we used are

$$\mu = (1.0, 1.25, 1.50, 1.75, 2.0, 2.25, 3.0, 6.0, 9.0, 12.0), \tag{17a}$$

$$\mu_0 = (1.0, 1.25, 1.50, 1.75, 2.0, 2.25, 3.0, 6.0, 9.0, 12.0). \tag{17b}$$

TABLE 2. Satellite sensor channels that we recommend using Planck-weighted transmittance; n16, n17, n18, n19: NOAA family satellites 16, 17, 18, and 19, respectively; metop-a: The Meteorological Operational Satellite A; m08, m09, m10: Meteosat serials 8, 9, and 10; aatsr: Advanced Along-Track Scanning Radiometer; envisat: Environmental Satellite; atsr: Along Track Scanning Radiometer; ers1, ers2: European Remote Sensing Satellite series 1 and 2; imgr: Imager; g12, g13, g14: Geostationary Operational Environmental Satellites series 12, 13, and 14; mt1r, mt2: Multifunctional Transport Satellites 1R and 2.

			BT band correction coefficients		
Satellite sensor/channel	Spectral interval (cm^{-1})	Central wavenumber (cm^{-1})	b	b_1	Rank
avhrr3_n16 channel 3	2222.7–3355.7	2697.562	2.2687×10^{0}	9.9642×10^{-1}	9
avhrr3_n17 channel 3	2418.4–2947.2	2670.800	1.7251×10^{0}	9.9771×10^{-1}	5
avhrr3_n18 channel 3	2406.2–2977.9	2663.004	1.7627×10^{0}	9.9767×10^{-1}	6
avhrr3_n19 channel 3	2418.4–3034.9	2671.660	1.7074×10^{0}	9.9773×10^{-1}	4
avhrr3_metop-a channel 3	2382.1–3041.3	2689.894	2.1320×10^{0}	9.9720×10^{-1}	8
seviri_m08 channel 4	2224.1–2913.2	2566.019	3.3476×10^{0}	9.9540×10^{-1}	15
seviri_m09 channel 4	2083.3–3289.5	2568.259	3.3855×10^{0}	9.9540×10^{-1}	16
seviri_m10 channel 4	2213.8–2947.1	2565.885	3.3204×10^{0}	9.9547×10^{-1}	14
aatsr_envisat channel 1	2176.1–3120.5	2680.398	1.8322×10^{0}	9.9747×10^{-1}	7
atsr1_ers1 channel 3	2426.1–3099.8	2693.365	2.3416×10^{0}	9.9693×10^{-1}	10
atsr2_ers2 channel 3	2251.2–3293.9	2727.513	2.8438×10^{0}	9.9614×10^{-1}	13
imgr_g12 channel 2	2419.1–2670.0	2564.822	6.9902×10^{-1}	9.9902×10^{-1}	1
imgr_g13 channel 2	2002.5–3333.5	2563.957	1.4800×10^{0}	9.9794×10^{-1}	2
imgr_g14 channel 2	2227.1–2852.0	2573.925	1.5567×10^{0}	9.9783×10^{-1}	3
imgr_mt1r channel 5	2381.7–3029.1	2653.665	2.3479×10^{0}	9.9697×10^{-1}	11
imgr_mt2 channel 4	2466.0–2908.9	2684.116	2.4637×10^{0}	9.9678×10^{-1}	12

The total solar transmittances and PW1 total transmittances for the UBMC 48 profiles are calculated in LBLRTM, so that for each channel, we have 480 (10 angles × 48 profiles) total transmittances pairs. Figure 11 shows a scatterplot of PW1 total transmittances against total solar transmittances for *Meteosat-9* SEVIRI channel 4. After regression, the predicted solar transmittances against the true solar transmittances are shown in Fig. 12. It is demonstrated that the multiple regression method can be used to accurately predict the solar transmittance. The coefficients and correlations for these 16 channels are given in Table 3.

Without considering the correction of the difference between PW1 total transmittance and total solar transmittance, the radiance error ΔR_{sol} was calculated from Eq. (15). We then replaced the PW1 total transmittance with the predicted total solar transmittance from Eq. (16) and recalculated ΔR_{sol} after the correction. The radiance error ΔR_{sol} can be converted to the BT error (ΔBT_{280}, with respect to an effective brightness temperature of 280 K) using the radiance derivative of Eq. (10) with respect to $T_e = 280$ K. Figure 13 summarizes the statistics for solar reflection both before and after the solar correction with typical surface reflectivities of 0.01 and 0.1 for the UMBC 48 profiles and 10 angles. After the correction, the biases and standard deviations are dramatically reduced, compared to those without the correction.

6. Conclusions

In this study, three approximation methods are applied to calculate the level-to-space transmittances that are used to generate coefficients for fast radiative transfer models. The approximations are tested against the LBL results for a chosen five infrared broadband channels. Among them, four channels are in the NIR and one is in around the 15-μm CO_2 absorption region.

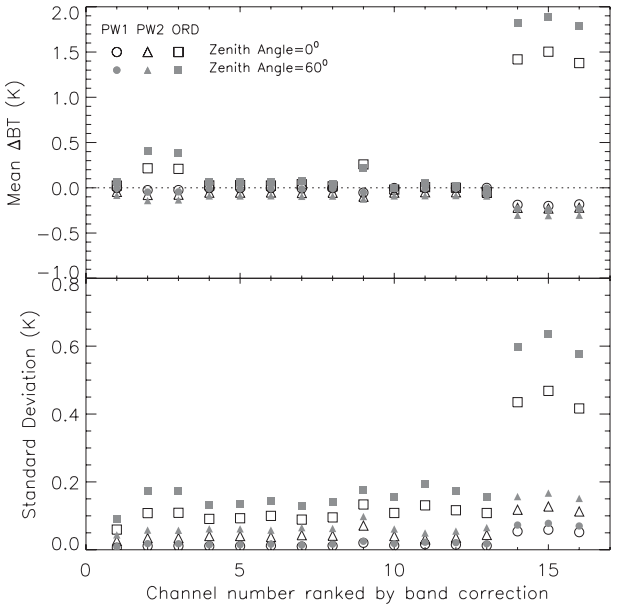

FIG. 10. Mean brightness temperature differences and standard deviations for approximation methods PW1, PW2, and ORD compared to LBL results for the UMBC 48 diverse atmospheric profiles at nadir for the satellite sensor channels shown in Table 2.

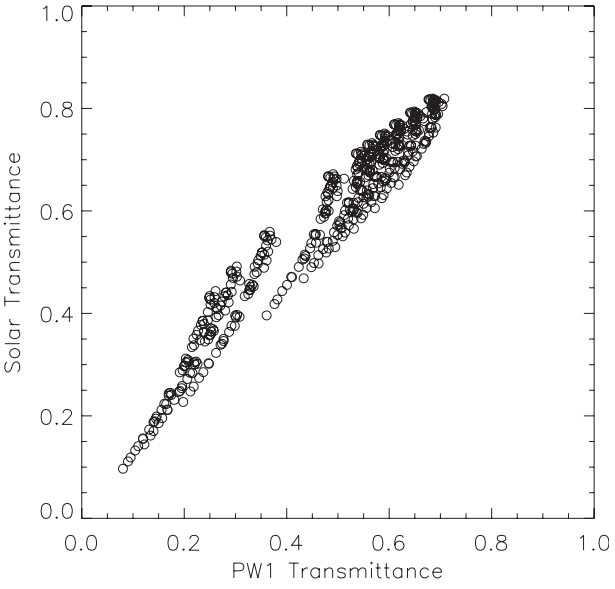

FIG. 11. Scatterplot of PW1 total transmittance against total solar transmittance for *Meteosat-9* SEVIRI channel 4.

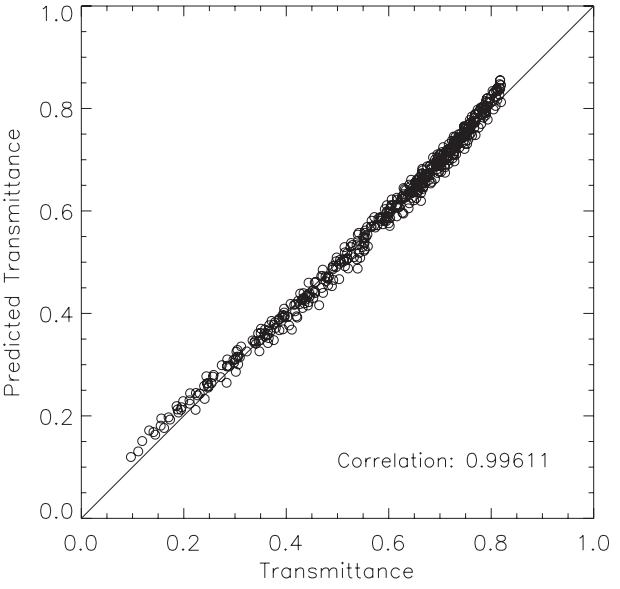

FIG. 12. Predicted solar transmittances from PW1 transmittances vs solar transmittances for *Meteosat-9* SEVIRI channel 4.

Two channels have very broad SRFs. Comparison results show that when the channel spectral response function is very broad (i.e., the band correction coefficient b is greater than 1.0 K), we should consider applying a Planck-weighted transmittance approximation instead of the ordinary transmittance approach in fast models (note that RTTOV has made use of PW transmittance since 2003). Under all circumstances, the effective layer temperature Planck-weighted approximation is better than using the level temperature Planck-weighted approximation. The Planck-weighted methods are more sensitive to atmospheric and surface temperatures than the ORD method. When the surface temperature increases, the bias from the PW methods generally increases, while the ORD method shows more consistent results. For channels 2 and 4, the PW methods can capture the second weight function peak near 20 hPa because of the strong 4.3-μm CO_2 absorption and the larger variation of Planck radiance at those wavenumbers.

Three layer schemes are used to test the sensitivity of the three methods to the profile vertical structure. For a coarser vertical stratification of atmospheric profiles, which has a large temperature difference between the

TABLE 3. Multiple linear regression coefficients and correlations for predicting the total solar transmittance.

Satellite sensor/channel	β_0	β_1	β_2	β_3	Corr
avhrr3_n16 channel 3	5.3048×10^{-2}	1.0566×10^{0}	1.8296×10^{-3}	-3.2228×10^{-4}	0.998 68
avhrr3_n17 channel 3	1.5507×10^{-2}	1.0785×10^{0}	5.0768×10^{-3}	-3.0020×10^{-4}	0.999 68
avhrr3_n18 channel 3	1.9030×10^{-2}	1.0866×10^{0}	5.8142×10^{-3}	-3.3395×10^{-4}	0.999 58
avhrr3_n19 channel 3	1.4448×10^{-2}	1.0763×10^{0}	4.9270×10^{-3}	-2.8999×10^{-4}	0.999 70
avhrr3_metop-a channel 3	1.3254×10^{-2}	1.0771×10^{0}	4.6724×10^{-3}	-2.9042×10^{-4}	0.999 75
seviri_m08 channel 4	6.1331×10^{-1}	9.9189×10^{-1}	-6.9600×10^{-4}	-1.7916×10^{-3}	0.996 30
seviri_m09 channel 4	6.2411×10^{-1}	9.7648×10^{-1}	-9.0409×10^{-4}	-1.8103×10^{-3}	0.996 11
seviri_m10 channel 4	6.1775×10^{-1}	9.8030×10^{-1}	-9.2891×10^{-4}	-1.7911×10^{-3}	0.996 23
aatsr_envisat channel 1	1.8507×10^{-2}	1.0719×10^{0}	4.5444×10^{-3}	-2.8641×10^{-4}	0.999 74
atsr1_ers1 channel 3	1.8704×10^{-2}	1.0752×10^{0}	4.7100×10^{-3}	-3.1429×10^{-4}	0.999 74
atsr2_ers2 channel 3	1.3698×10^{-2}	1.0600×10^{0}	3.2383×10^{-3}	-2.5877×10^{-4}	0.999 88
imgr_g12 channel 2	1.0252×10^{-1}	1.0289×10^{0}	3.9579×10^{-3}	-4.5228×10^{-4}	0.999 56
imgr_g13 channel 2	3.3497×10^{-1}	9.6491×10^{-1}	1.3638×10^{-3}	-1.0065×10^{-3}	0.998 41
imgr_g14 channel 2	3.0687×10^{-1}	9.9298×10^{-1}	3.1110×10^{-3}	-9.9705×10^{-4}	0.998 25
imgr_mt1r channel 5	4.6493×10^{-2}	1.1132×10^{0}	8.2331×10^{-3}	-5.2701×10^{-4}	0.999 18
imgr_mt2 channel 4	5.3643×10^{-3}	1.1048×10^{0}	6.6822×10^{-3}	-3.5728×10^{-4}	0.999 57

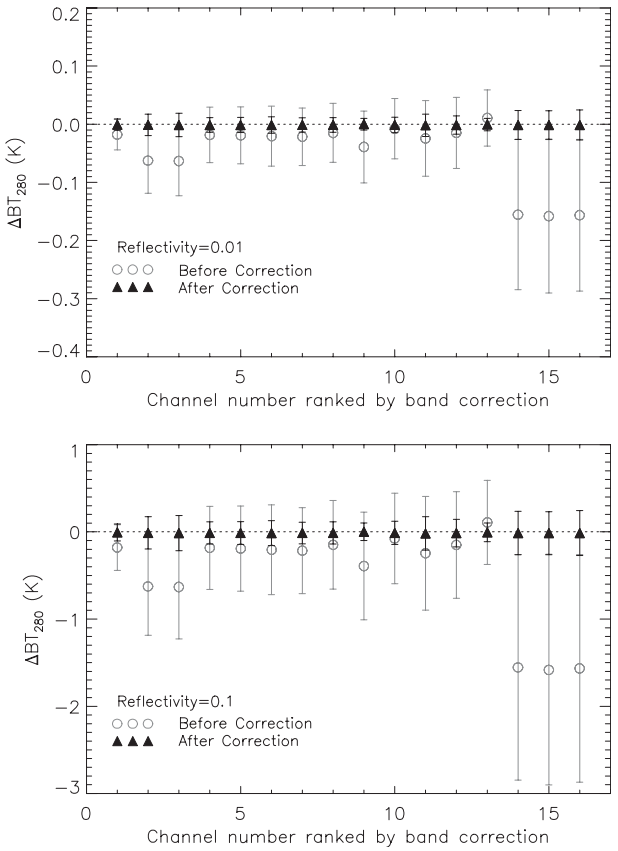

FIG. 13. Statistics for solar reflection before and after correction with reflectivity of (top) 0.01 and (bottom) 0.1. The biases for before (open circles) and after (solid triangles) correction are shown. The standard deviations are also shown (vertical bar).

levels, the impact from PW1 on the radiance is much smaller than PW2. The absolute bias increases when the vertical resolution is getting coarser. However, the BT double differences show that PW1 is much better than PW2 and ORD and closely follows the LBL results.

Based on these simulations and comparisons, when the band correction for channel brightness temperature is smaller, especially when coefficient b is less than 1, the ORD method should be used to calculate the transmittance instead of Planck-weighted transmittances because of the consistent BT differences to LBL. When the band correction coefficient b is greater than 1, the PW1 method should be used to take account of the Planck radiance variation with the transmittance within the band spectra to reduce the larger BT differences when using the ORD method.

When considering the solar contribution in daytime, the correction of the solar reflection has been made for near-infrared broadband channels when using the PW1 transmittance. The solar transmittance is predicted by using explanatory variables such as the PW1 transmittance, secant of zenith angle, and surface temperature. With this correction, the error reduces to a more reasonable level. With PW1 method and solar reflection correction in fast radiative transfer models, the accuracy for radiance simulation can be improved for the very broadband satellite infrared channels.

Acknowledgments. The authors thank David Groff for his detailed corrections and comments. Thanks also extended to Dr. Xingming Liang for his internal review, and two anonymous reviewers for their very useful suggestions to improve our paper. This research was supported by Chinese Ministry of Science and Technology under 973 Project 2010CB951600 and the Joint Center for Satellite Data Assimilation program. The contents of this paper are solely the opinions of the author(s) and do not constitute a statement of policy, decision, or position on behalf of NOAA or the U.S. Government.

REFERENCES

Berk, A., 2008: Analytically derived conversion of spectral band radiance to brightness temperature. *J. Quant. Spectrosc. Radiat. Transfer,* **109,** 1266–1276.

Brunel, P., and S. Turner, 2003: On the use of Planck-weighted transmittances in RTTOV. International TOVS Working Group Poster, *13th Int. TOVS Study Conf.,* Ste Adele, QC, Canada. [Available online at http://cimss.ssec.wisc.edu/itwg/itsc/itsc13/thursday/brunel_poster.pdf.]

Chen, Y., F. Weng, Y. Han, and Q. Liu, 2008: Validation of the Community Radiative Transfer Model (CRTM) by using CloudSat data. *J. Geophys. Res.,* **113,** D00A03, doi:10.1029/2007JD009561.

——, Y. Han, P. van Delst, and F. Weng, 2010: On water vapor Jacobian in fast radiative transfer model. *J. Geophys. Res.,* **115,** D12303, doi:10.1029/2009JD013379.

Chevallier, F., S. D. Michele, and A. P. McNally, 2006: Diverse profile datasets from the ECMWF 91-level short-range forecast. NWP SAF Rep. NWPSAF-EC-TR-010, 16 pp. [Available online at http://research.metoffice.gov.uk/research/interproj/nwpsaf/rtm/profiles_91L.pdf.]

Chou, M. D., and K. T. Lee, 2005: A parameterization of the effective layer emission for infrared radiation calculations. *J. Atmos. Sci.,* **62,** 531–541.

Clough, S. A., M. W. Shephard, E. J. Mlawer, J. S. Delamere, M. J. Iacono, K. Cady-Pereira, S. Boukabara, and P. D. Brown, 2005: Atmospheric radiative transfer modeling: A summary of the AER codes. *J. Quant. Spectrosc. Radiat. Transfer,* **91,** 233–244.

Han, Y., P. van Delst, Q. Liu, F. Weng, B. Yan, R. Treadon, and J. Derber, 2006: Community Radiative Transfer Model (CRTM), version 1. NOAA Tech. Rep. NESDIS 122, 40 pp.

Liu, Q., X. Liang, Y. Han, P. van Delst, Y. Chen, A. Ignatov, and F. Weng, 2009: Effect of out-of-band response in *NOAA-16* AVHRR channel 3B on top-of-atmosphere radiances calculated with the Community Radiative Transfer Model. *J. Atmos. Oceanic Technol.,* **26,** 1968–1972.

Matricardi, M., 2008: The generation of RTTOV regression coefficients for IASI and AIRS using a new profile training set and a new line-by-line database. ECMWF Research Dept. Tech. Memo. 564, pp. [Available online at http://www.ecmwf.int/publications/library/ecpublications/_pdf/tm/501-600/tm564.pdf.]

McMillin, L. M., X. Xiong, Y. Han, T. J. Kleespies, and P. Van Delst, 2006: Atmospheric transmittance of an absorbing gas. 7. Further improvements to the OPTRAN 6 approach. *Appl. Opt.,* **45,** 2028–2034.

Saunders, R. M., and Coauthors, 2007: A comparison of radiative transfer models for simulating Atmospheric Infrared Sounder (AIRS) radiances. *J. Geophys. Res.,* **112,** D01S90, doi:10.1029/2006JD007088.

——, M. Matricardi, and P. Brunel, 1999: An improved fast radiative transfer model for assimilation of satellite radiance observation. *Quart. J. Roy. Meteor. Soc.,* **125,** 1407–1425.

Strow, L. L., S. E. Hannon, S. D. Souza-Machado, H. E. Mottler, and D. Tobin, 2003: An overview of the AIRS radiative transfer model. *IEEE Trans. Geosci. Remote Sens.,* **41,** 303–313.

Weinreb, M. P., H. E. Fleming, L. M. McMillin, and A. C. Neuendorffer, 1981: Transmittances for the TIROS Operational Vertical Sounder. NOAA Tech. Rep. NESS 85, 69 pp. [Available online at http://docs.lib.noaa.gov/rescue/TIROS/QC8795U45no85.pdf.]

Weng, F., Y. Han, P. van Delst, Q. Liu, and B. Yan, 2005: JCSDA community radiative transfer model (CRTM). *Proc. 14th Int. ATOVS Study Conf.,* Beijing, China, International TOVS Working Group, 217–222.